Science Advances
AAAS

Supplementary Materials for

'Depths in a day - A new era of rapid-response Raman-based barometry using fluid inclusions'

*Charlotte L. DeVitre *et al.*

*Corresponding author. Email: cl.devitre@gmail.com

This PDF file includes:

Other Supplementary Materials for this manuscript include the following:

Data S2 and S3:
- S2 is the fluid inclusion dataset
- S3 is the global melt inclusion compilation

S4 FI Navigation Image Compilation
S5 Email and tracking record

All other raw data (spectra, metadata, FI images) as well raw Jupyter processing notebooks can be found on a Github repository (https://github.com/cljdevitre/2023_Kilauea-rapid-response-simulation) which will be archived at Zenodo upon acceptance.

Supplementary Text

Sample collection and preparation

Tephra samples (USGS code KS23-588) representing the first ~14 hours of the September 10, 2023, eruption of Kīlauea volcano were collected by Hawaiian Volcano Observatory (HVO) geologists on September 12 and shipped on Friday September 15 at ~5 pm HST. This tephra was erupted from a fissure which opened at 15:36 local time on September 10 (~22 minutes after the eruption started, between 15:13 and 15:14 local time) and ceased erupting between 06:16 and 06:18 am local time on September 11. Following receipt of the samples at the University of California, Berkeley on Tuesday, September 19, material was processed in a jaw crusher in the VIBE lab which was thoroughly cleaned the week before and the morning of the simulation, and then sieved into >2 mm, 1–2 mm, and 0.5–1 mm size fraction. Crystals were picked from the 1–2 mm and 0.5–1 mm size fraction using three different binocular microscopes (one of which had the ability to cross polars). Then, crystals were individually mounted in CrystalBond™ on glass slides and progressively polished with 1200-2500-10000 grade wet and dry paper to find FI. Grains containing FI were then passed onto a team member on a research grade scope to take reflected and transmitted light images to aid with Raman navigation. These images were pasted into a Google slides document so all lab personnel at UC could access them immediately (images are compiled in supplement S4 FI Image Compilation as an example).

A lava flow sample (USGS code KS23-587) was collected in a molten state and quenched with water at 6:30 AM HST on the 11 of September 2023. The sample was entirely glassy, and fragments were mounted in a 1" epoxy round and polished for microprobe analysis.

Raman analyses

Raman spectra were acquired using a WiTec Alpha 300R Raman spectrometer at the Department of Earth and Planetary Science at the University of California, Berkeley. The relationship between CO_2 density and spectral features was determined from a gas calibration cell following the methods of(*1*). All spectra were acquired from samples heated to 37 °C. Spectra were processed and corrected for drift using the Python tool DiadFit v0.0.73. We report ratios of SO_2 to CO_2 peak areas. We filtered the final dataset for SO_2/CO_2 ratio < 0.22 (Fig. 2d), to ensure use of the pure CO_2 EOS was valid (Given an instrumental efficiency of 1 for our Raman, this corresponds to <10 mol% SO_2). No fluid inclusions contained carbonate peaks nor any gaseous species other than CO_2. We calculated densities from the Raman-measured separation of the Fermi diad using the appropriate calibrated density equations for our instrument in DiadFit (*2*). For the final dataset (Day 4), we took a mean of duplicate analyses, and calculated pressures using the EOS of (*3*) using an entrapment temperature estimated from the Fo content close to the FI (*1*). Entrapment depths in Fig. 2d were calculated using a constant crustal density of 2300 kg/m^3 and a normally distributed 1$\boldsymbol{\sigma}$ error of 100 kg/m^3. Error in the CO_2 density for each FI was determined from the error in each peak fit, the Ne line drift correction model, and the densimeter (*2*). We used a 40°C error for temperature (*1*). We propagated these three sources of uncertainty in FI depths using MonteCarlo simulations implemented in DiadFit v 66. In total we analyzed 62 FI hosted in 31 olivine crystals. Our workflow is detailed in Fig. 2 of the main text. Pictures of each FI and host crystal are available in the repository linked at the beginning. We note here that the initial data reported for Days 1 and 2 did not account for repeated analyses (1 repeated FI in Day 1 and 6 in

Day 2; we took a mean of repetitions on Day 4), pressures were calculated using an estimated entrapment temperature of 1150˚C (*1*, *4*), and depth was calculated using the crustal density model in (*5*, *6*).

Epoxy mount making and polishing

After Raman analysis, crystals were removed from CrystalBond™* using a hotplate and placed in Acetone. They were then mounted on double-sided sticky tape with their polished side down. EpoFix™* resin was used to impregnate the samples in a Cast-N-Vac vacuum pourer. After curing, the epoxy mount was polished using an EcoMet30 automatic polisher, with 9, 3, and 1 um diamond pastes. A reflected light map and image of each crystal was taken using the Raman microscope to aid SEM sample navigation. The location within each FI in the reflected light image was cataloged so the Scanning Electron Microscope (SEM) operator knew where to analyze to obtain an approximate Fo content for each FI.

EDS analysis

Samples were carbon coated to an approximate thickness of 25–30 μm for EDS analysis. Chemical data for each host crystal in the proximity of each FI was determined using a Zeiss EVO MA-10 SEM and a single AMETEK EDAX 10 mm^2 detector at the University of California, Berkeley. The beam was rastered over a 30-by-30 μm area for ~75–80s (a live time of 60 seconds with ~30% dead time). For all analyses we used an accelerating voltage of 20 kV and a 30 μm aperture, giving an approximate beam current of 5 nA. EDS data reduction was performed using an in-built standardless quantification routine (including a ZAF matrix correction), alongside pre-determined "Standardless Element Coefficients" (SECs). The SECs act as correction factors for each element in the standardless quantification routine and have been determined through several years of repeat analyses of multiple different silicate standard materials and glasses. This method returns an estimate for the relative abundance of each element in the analyzed material and, if a normalization to 100% is assumed, can be used to return semi-quantitative chemical analysis of elemental or oxide weight percent values. However, for the purposes of this study we simply focused on the relative abundance of Mg and Fe in the EDS analyses to calculate the Fo content of the olivine host crystals. Furthermore, by calculating the molar Si/(Mg+Fe) ratio of each analysis we were able to provide a stoichiometric check of data quality: we obtained an average Si/(Mg+Fe) ratio of 0.497±0.006 on Kīlauea olivine crystals, close to the ideal value of ~0.5. Precision and accuracy were determined through repeat measurements of the San Carlos and Springwater olivines, which were not used as part of the standard quantification routine. We estimate the precision and accuracy of the method using repeat analyses of secondary standards (5 at start, 5 at end of day), which have Fo contents similar to our samples (see supplementary dataset S2). The Smithsonian-preferred Fo content (*7*) for the San Carlos secondary standard is 90.2 Fo, and we obtained a mean of 89.84±0.07 Fo units. For Springwater, the preferred value is 82.4 Fo, and we obtained a mean of 82.1±0.2 Fo. We also analyzed a Kīlauea olivine crystal previously measured on the USGS Menlo Park EPMA. The average Fo content obtained at Menlo Park was 87.8±0.1 Fo units, and at the University of California, Berkeley SEM, 88.5±0.1. It should be noted that such offsets also exist between different EPMA labs (*8*). Considering these probable differences, we compared data acquired at Stanford University to that obtained at Cambridge University on the olivine crystals of (*4*). The difference observed amounts to ~0.62 units at ~82

Fo and 0.78 units at 90 Fo (*1*). Thus, EDS errors are within uncertainty of offsets between different microprobe labs.

EPMA analysis of glasses

Major and minor element analysis of glass from USGS sample KS23-587 was done using the U.S. Geological Survey's JEOL 8530F microprobe at the California Volcano Observatory. The samples were run over midnight between September 23 and 24th, 2023, in 1hr 37 minutes (9/23/2023 23:06 - 9/24/2023 0:43). A total of 20 total analyses were conducted, corresponding to 4 analyses per grain in 5 grains. These samples were run as part of a pre-booked session for other samples that started on September 20th. We note however that CalVO microprobe personnel later informed us that it would be possible in the future to request immediate access for eruption response if needed. This would mean that a glass mount could be prepared in 24 hrs after sample collection, shipped within 2 days from HVO to CalVO and analyzed on the probe on day 4 post field collection (calibration takes 2-3 hrs and analysis ~2 hours). We also note that if these measurements did not exist at the time of the simulation, we could have used the EDS-SEM method to get the Mg# of the host glass to calculate the equilibrium olivine Fo content shown on Fig. 2 (The only reason we need this EPMA data). EDS measurements on the matrix glass were within 1-2 Mg# units of EPMA measurements – far smaller than the uncertainty associated with calculating an equilibrium olivine content based on uncertainty regarding the choice of olivine-liquid K_D model at Kīlauea.

Microprobe glass analyses used 15 kV accelerating voltage and a 10 μm beam with a 10 nA current. Peak counting times were 45 s for S, Cl, and F, 40 s for Ti, P, and Mn, 20 s for Si, Ca, Fe, Al, and Mg, and 10 s Na and K (backgrounds were measured on both sides of the peak for half the peak counting times). Standards were VG2 basaltic glass (USNM 111240/52;ref (*7*)) for Si, Mg, and Al, Kakanui Pyrope Garnet (USNM 143968) for Fe, and Al, Wollastonite for Ca, Tiburon Albite for Na, MnO_3 for Mn, TiO_2 for Ti, Orthoclase OR-1A for K, Wilburforce Apatite (USGS-M105731) for P, Barite for S, Sodalite for Cl, and MgF_2 for F. Two-sigma relative precision, based on two analyses of VG-2 glass (before and after lava sample was run), are 0.19 wt% for SiO_2, 0.15 wt% for Al_2O_3, 0.003 wt% for TiO_2, 0.27 wt% for FeO, 0.009 wt% for MnO, 0.006 wt% for MgO, 0.04 wt% for CaO, 0.11 wt% for Na_2O, 0.02 for K_2O, 0.04 for P_2O_5, 0.07 for SO_3, 0.0001 for Cl, and 0.002 for F. X-ray intensities were converted to concentrations using standard ZAF corrections(*9*). Analyses with totals <99.0 wt% or >100.5 wt% were rejected. Reported analyses are an average of four replicate points on individual glass fragments.

Manuscript Writing Timeline

The study presented here was formulated into a letter over days 4 and 5 (September 23-24th), sent to our co-authors on Day 6 (September 25th) and submitted for review to Nature Geoscience on Day 8 - September 27th, 2023 (see S5_Email_and_tracking_record for email confirmations), one week after we begun the simulation. Unfortunately, despite our prompt submission, we did not receive a rejection notification until a month later, owing to editorial delays. The rejection, based on the grounds of 'lack of appeal for the broader Geoscience community', was surprising, given the significant interest of the Geoscience community in hazard mitigation. We proceeded to submit the manuscript to PNAS on October 31st, 2023 (see S5_Email_and_tracking_record) who rejected the manuscript on November 15th (see S5) on similar grounds with the editor comments

as follows: “This is indeed an interesting real-time procedure but may be too specialized for PNAS”. After submitting to Journal of Petrology on November 16th, 2023, we received a rejection from JPET on January 19th, 2024, based on concerns from reviewers of temperature sensitivity of EOS and the lack of applicability to subduction zones (S5). We have addressed these concerns with the new Fig. 1 and Fig. 4 and further details in the supplement and body of the article and believe the new manuscript has significant global applicability, hence our submission to Science Advances. Regardless it is evident that the delays in the editorial and publishing process constitute possibly the biggest bottleneck for reporting findings to the community, particularly given USGS collaborations mean that results cannot be posted as preprints prior to peer review.

Identifying and Resolving Bottlenecks

The yellow stars on Fig. 1 identify current bottlenecks in the process that could be easily improved.

Star 1 – Shipping and receiving samples

Distributing samples to the University of California, Berkeley was not a top priority for HVO because this simulation was being attempted for the first time, and as a result, there was no guarantee of obtaining magma storage depths in a timely manner. Samples were shipped from Hilo on a Friday at ~5 pm HST. HVO was asked to ship samples to a private residence under the assumption that they might arrive over the weekend. However, no packages leave Hilo after 4pm on Friday over the weekend, so the samples started their transit to California on Monday. Had the package been taken to the courier’s office on Friday morning, it would likely have arrived on Sunday. The tracking information indicated arrival on Wednesday, which is when we planned to start the simulation. However, the samples arrived at the private residence on Tuesday morning during working hours, without notification that the package had been delivered (and no one was home).

We have demonstrated that this technique adds valuable quantitative depth information that expands on HVO’s routine near-real-time chemical monitoring with bulk rock ED-XRF(*10*). Under ideal circumstances, HVO geologists would sample tephra or molten lava from the eruption on Day 1 (morning) and dry the samples in the lab on Day 1 (afternoon), dropping the samples for shipment on the evening of Day 1, which would go out early on Day 2 (as long as the drop off did not occur Friday afternoon or over the weekend). Same-day shipping from Hawaii to California is not realistic, but samples shipping Monday through Thursday mornings would allow for arrival on Day 3. Additionally, it would be possible to get samples to the University of California, Berkeley within 24 hours if someone in Hawai’i were to take a flight to San Francisco or Oakland airport with the samples, or within ~30 hours if someone based in the University of California, Berkeley flew to Hawai’i, picked up the samples, and returned home immediately.

We note that this bottleneck can be avoided entirely if observatories rely on local research expertise (for example, in collaboration with local academic research groups) and/or establish in-house workflows for this type of work. In such a case, next-day information could readily be obtained. As this is not an option for HVO, the Hawaii-California connection will serve as the fastest way to conduct this rapid-response barometry.

Star 2 – Sample cataloging

The WITEC Raman microscope used in this study does not have a condenser in its optical path, which can make it difficult to navigate and find FIs directly, particularly in volcanic crystals that are commonly coated in glass. The first 7–10 crystals were analyzed immediately after preparation with no navigation photos, so finding the FI on the Raman scope added some time. After AB had finished crushing, sieving, and picking, he began taking photos on a research-grade scope to help the Raman operator find the FIs they were supposed to be analyzing. Late on Day 2, when students were not available, Wieser began photographing crystals holding her phone to the eyepiece of the teaching-collection reflected light and transmitted light microscopes. This provided enough textural context to easily find FIs on the Raman (See Image Compilation S4 in the repository linked in the beginning). The main advantage of using smartphones is that the person who found each FI could identify it, rather than passing it off to another person who then must work out where the FI is before photographing it. This would greatly reduce the number of people needed for the simulation, as we almost always had one person taking photos.

Star 3 – Epoxy impregnation

We used EpoFix™ epoxy in our laboratory because it gives low backgrounds during SIMS analysis. After pouring the epoxy at ~7 pm, it was removed from its mount at ~9 am the next morning. The epoxy was still noticeably soft (to the extent it cracked coming out of the mold). This meant that we could not start polishing immediately. Instead, we had to wait a further ~5 hours for it to cure sufficiently to polish. If fast-curing epoxies were available, it is very possible that a team member could have stayed, and polished and cataloged the sample overnight, allowing SEM analysis on Friday (Day 3) rather than Saturday.

Effect of H_2O on calculated pressures

The exsolved fluid phase in shallow magmatic systems like Kīlauea is not pure CO_2, but rather contains a proportion of H_2O. Fluid inclusion studies typically assume that H_2O has been lost and therefore the measured CO_2 density must be corrected based on the molar fraction of H_2O and molar ratios (see (*11*)). With this, pressures can be calculated using a mixed H_2O–CO_2 equation of state. Although it was not possible to implement these calculations during our simulation, a recent paper (*12*) made it possible to implement these corrections in DiadFit. We recalculated pressures for our fluid inclusions using mol fractions of H_2O in the exsolved fluid calculated based on the polynomial equations for Kīlauea in ref (*1*). We iterated measurements 5 times and show X_{H_2O} calculated on Fig S1; the data for iteration 5 is reported in the full FI dataset (Dataset S2) and the jupyter notebook is available in the repository linked in the beginning. We note that for all 3 days, the mean and median correction factor is ~10%. Most FI have correction factors <20%. These correction factors do not shift our FI from one reservoir to another, therefore they do not affect the interpretation of our results.

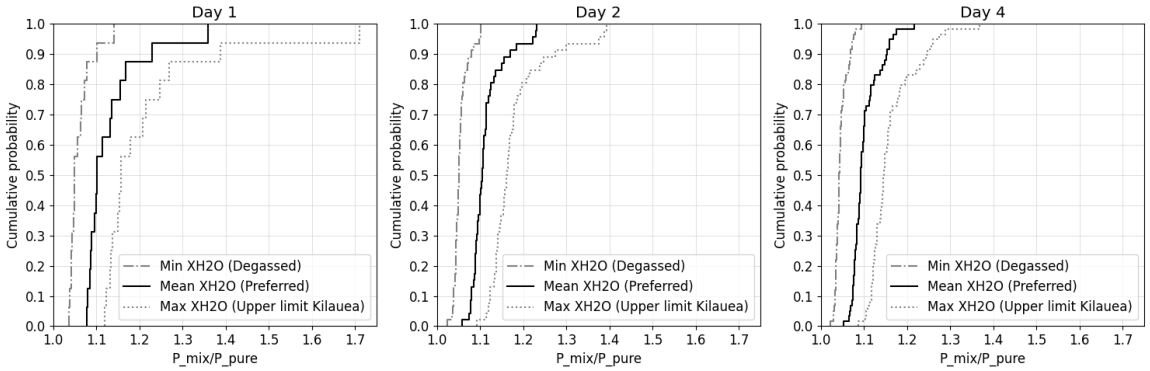

Fig. S1. Cumulative probability plot of the ratio of pressures from the mixed fluid EOS and pure CO_2 EOS depending on the X_{H_2O} function applied from (*1*) for each Day of the simulation.

Sensitivity of the EOS method for FI to entrapment temperature – Extended

We test the sensitivity of 3 equations of state for CO_2 available in DiadFit: two are for pure CO_2 (*3*, *13*) and one for CO_2-H_2O mixtures (*14*). For this, we calculated pressures using all three EOS at different magmatically relevant entrapment temperatures (for the mixed H_2O-CO_2 EOS we used X_{H_2O} = 0.1) which encompass the entire range of measured ol-saturated liquid temperatures at Kīlauea volcano (1100,1150, 1240 and 1350 ˚C). Overall, neither of the three equations of state are significantly sensitive to temperature at these magmatic temperatures (Fig. S2-S5). The shaded box in Fig. S2 shows storage conditions relevant to Kilauea. In the worst case, at the depth of the HMM reservoir (1 km), the absolute uncertainty in depth due to temperature is ~0.15 km and at depths corresponding to the SC reservoir (~4 km) it is ~0.7 km. We plot in detail on Figs S3-S5 the temperature sensitivity for each of the EOS at general conditions and conditions specifically relevant to Kīlauea volcano.

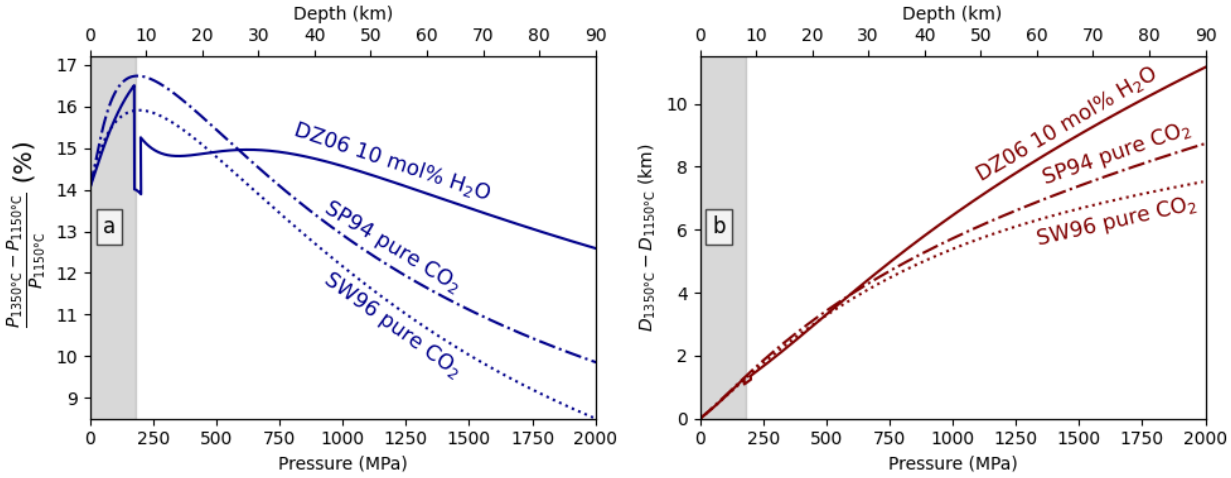

Fig. S2. % Difference in pressure (a) and absolute difference in depths (b) for pressures calculated at 1350˚C and 1150˚C using two pure CO_2 EOS (SW96 (*3*), SP94 (*13*)) and one mixed H_2O-CO_2 EOS (DZ06 (*14*)). Shaded area a indicates the range of pressures and depth relevant to Kīlauea pre-eruptive magma storage.

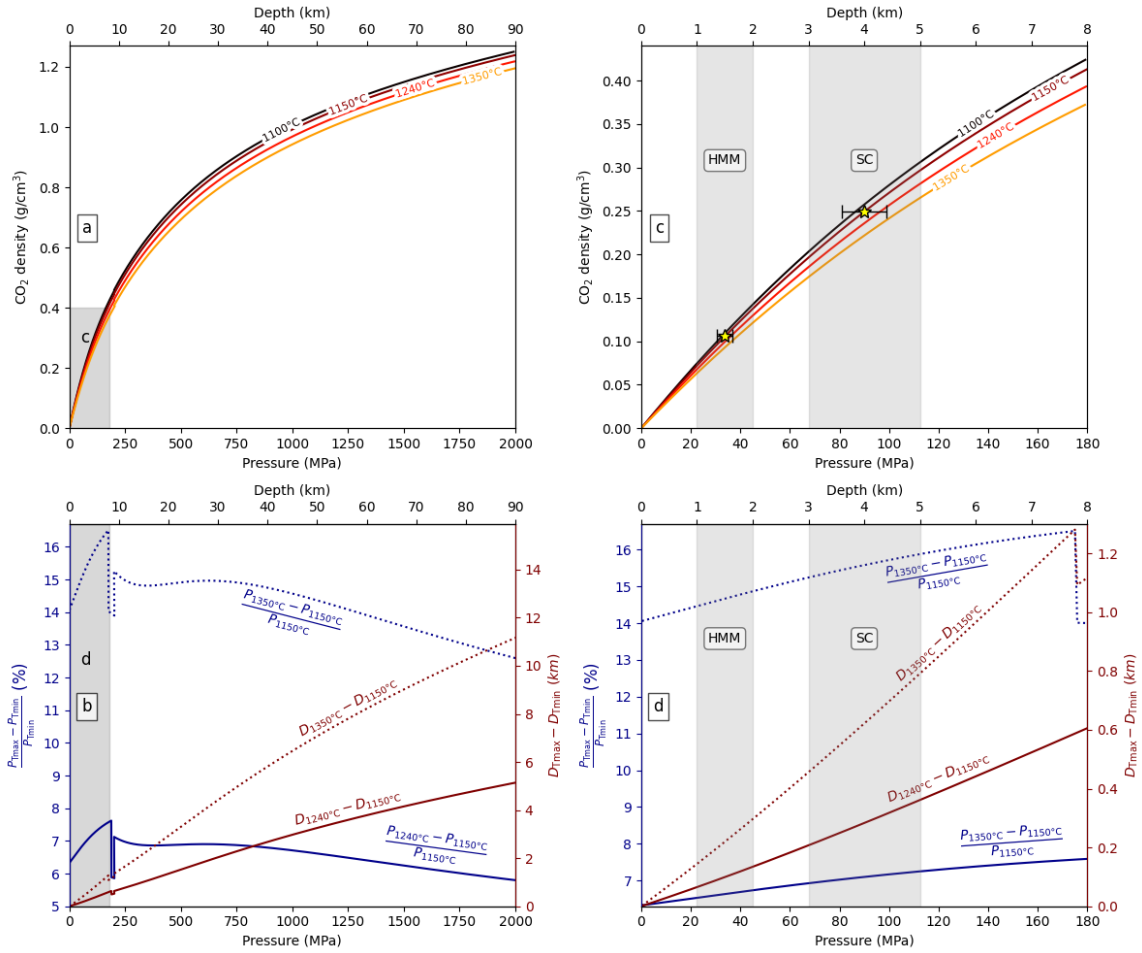

Fig. S3. Temperature sensitivity of the mixed CO_2-H_2O equation of state at 0.1 mol% H_2O (*14*). (a) Pressure vs CO_2 density calculated for various entrapment temperatures relevant at Kīlauea volcano. 1150 ˚C was our initial fixed temperature for days 1 and 2, 1240 ˚C is the rounded mean and median of all measured temperatures in our final dataset. (b) Depth and Pressure differences induced by uncertainty in temperature. Blue curves show the % difference in pressure (or depth) and maroon curves show the absolute difference in depth in km. (c) Closeup of panel a, representing relevant PT conditions for Kīlauea volcano. Grey boxes show the depth range of the magma storage reservoirs – HMM for Halema'uma'u and SC for South Caldera – inferred from FI and MI barometry as well as geophysics (*1*, *15*). Stars show hypothetical FI trapped at HM and SC reservoirs with error bars representing 1σ uncertainty from Monte Carlo simulations using a temperature uncertainty of ±150 K. (d) Closeup of panel b, showing depth and pressure differences induced by uncertainty in temperature for PT conditions relevant to Kīlauea volcano. Blue curves show the % difference in pressure (or depth) and maroon curves show the absolute difference in depth in km.

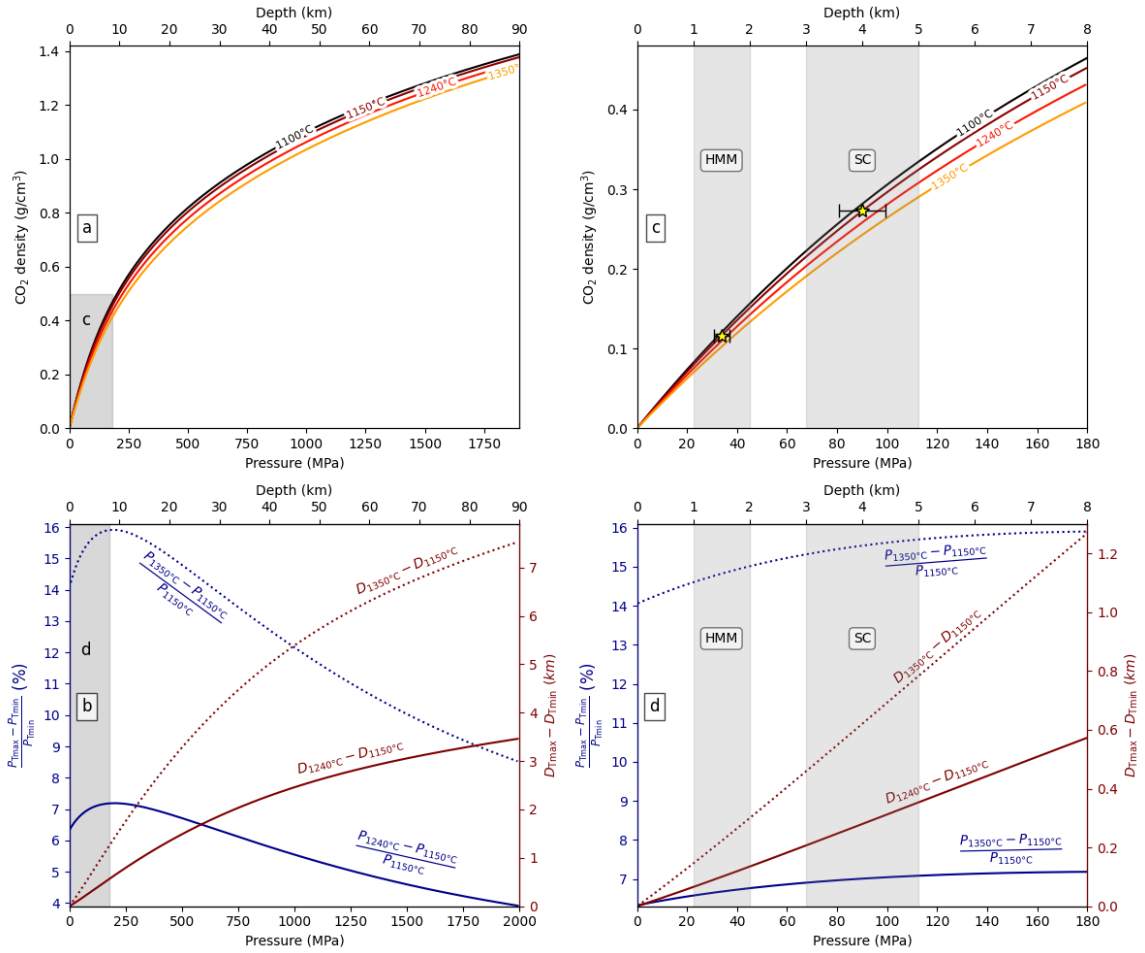

Fig. S4. Temperature sensitivity of Span and Wagner 1996 pure CO_2 equation of state (*3*).

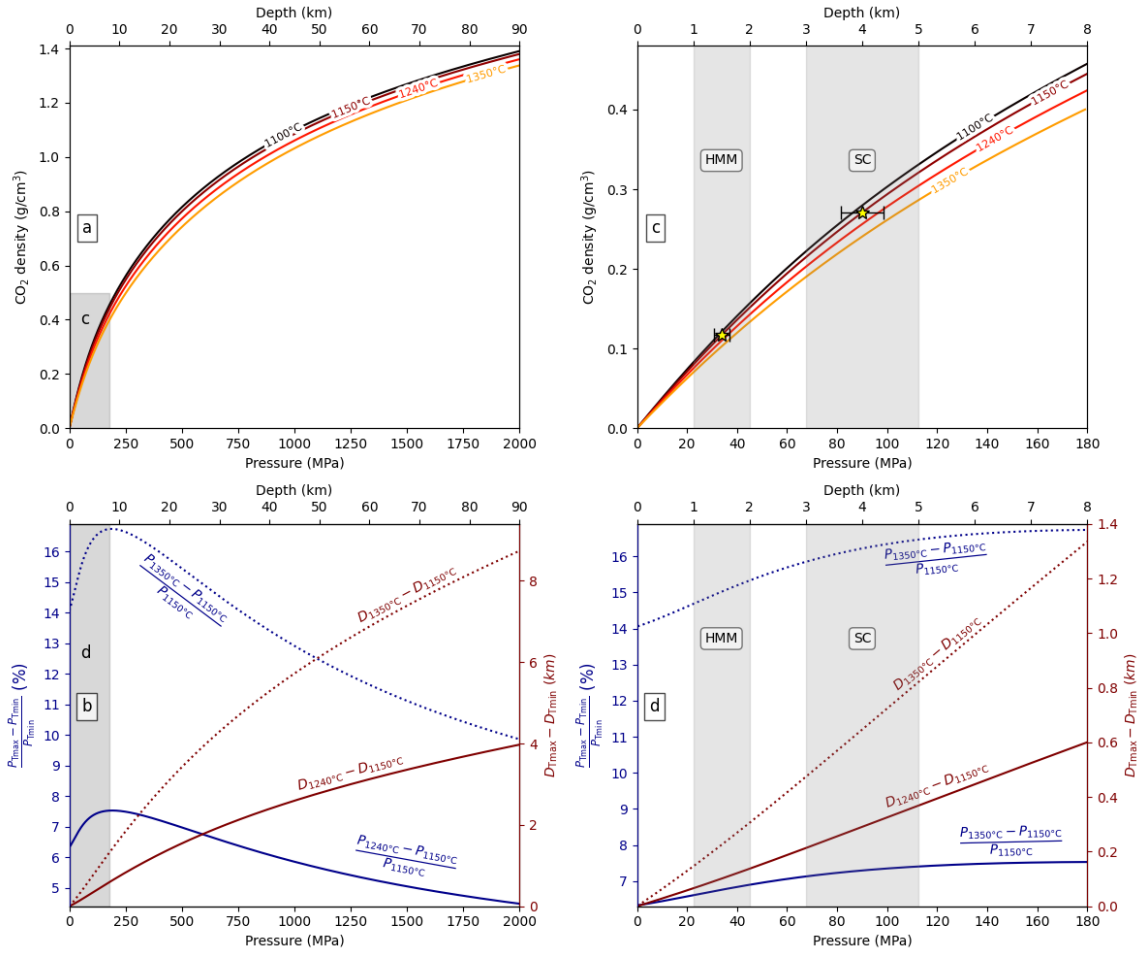

Fig S5. Temperature sensitivity of Sterner and Pitzer 1994 pure CO_2 equation of state (*13*).

Global Melt inclusion compilation

We compiled melt inclusion datasets with published major element data, H_2O and CO_2 concentrations in the glass from EarthChem (https://www.earthchem.org/), Georoc (https://georoc.eu/), (*16*)), (*17*) and (*18*)) as well as other MI datasets from the literature (*4*, *5*, *17*, *19–100*).

We calculated saturation pressures and the fraction of H_2O in the exsolved fluid phase (X_{H_2O}) using the MagmaSat solubility model (*101*) implemented in VESIcal (*102*). Whenever measurements were available, we used total CO_2 contents calculated from mass balance for Raman measured MI bubbles, otherwise we use glass-only CO_2. Also, when possible, we use post-entrapment crystallization corrected MI concentrations. As a first approximation, temperatures were calculated from major element data using the CaO liquid-only thermometer of (*103*) implemented in Thermobar (*104*) as it is not pressure sensitive and from there we calculated saturation pressures using MagmaSat. After this initial step, we recalculated temperatures using those pressures with the more appropriate ol-liq equation 22 of (*105*), coupled to a theoretical calculation of the D_{Mg} from (*106*), to calculate equilibrium olivine compositions so that equation 22 of (*105*) can be used as a liquid-only thermometer, as we did not have access to olivine pair chemistry (this is function "T_Put2008_eq22_BeattDMg" in Thermobar (*104*)). This equation has recently been identified as the most robust liquid-only thermometer across a wide range of compositions (*107*). After this, we recalculated saturation pressures using MagmaSat and our refined temperatures. We did not recalculate saturation pressures, temperatures or X_{H_2O} for MI in the Cascades compilation of (*18*). It is a known issue that MagmaSat may fail to converge and/or crash during saturation pressure calculations, which can be problematic when calculating saturation pressures on large datasets such as our >4000 MI compilation. To circumvent crashing issues, we implemented a python multiprocessing routine along with a try-except block using the python package "multiprocessing". The dataset was first divided in small chunks of ~20 samples and assigned to each processor core (in the case of this study a Dell Inspiron 15 with i7 8 core processor) limited to a maximum of 8 processes run simultaneously (as the author's laptop has 8 cores, so one process per core at a time). Within each ~20 sample chunk, the MI were run one by one within a try-except block such that whenever an error occurred, NaN values were returned along with the error message from VESIcal (*102*). Any MI for which MagmaSat did not converge were filtered out in the final dataset and the notebook is included in the data repository linked in the beginning. We provide both the complete unfiltered X_{H_2O} compilation, and the compilation filtered for MagmaSat errors, SiO_2 < 57 wt% and MgO < 16 wt%. As discussed in previous sections, our method is not applicable to systems and magmas where X_{H_2O} is very high, like for example in high silica magmas where H_2O is concentrated due to fractional crystallization and CO_2 is lost due to extensive degassing. Therefore, we plot only mafic MI with SiO_2 < 57 wt% (Fig. S7), likely representative of recharge magmas regardless of tectonic setting and for which the method could be applicable to determine locations in the world where the method could be relevant. Interestingly, it is evident that X_{H_2O} tends to be higher at alkaline intraplate volcanoes than their tholeiitic counterparts at similar pressures (Fig. S8).

We then plot X_{H_2O} against pressure at each unique location, grouped by tectonic settings (Fig. S9a-e). It is notable that there is a marked increase in X_{H_2O} at very low pressures (<50 MPa). We filter the dataset presented on Fig 4, and Fig S10 considering a pressure cutoff of 20 MPa, where X_{H_2O} is very high regardless of setting.

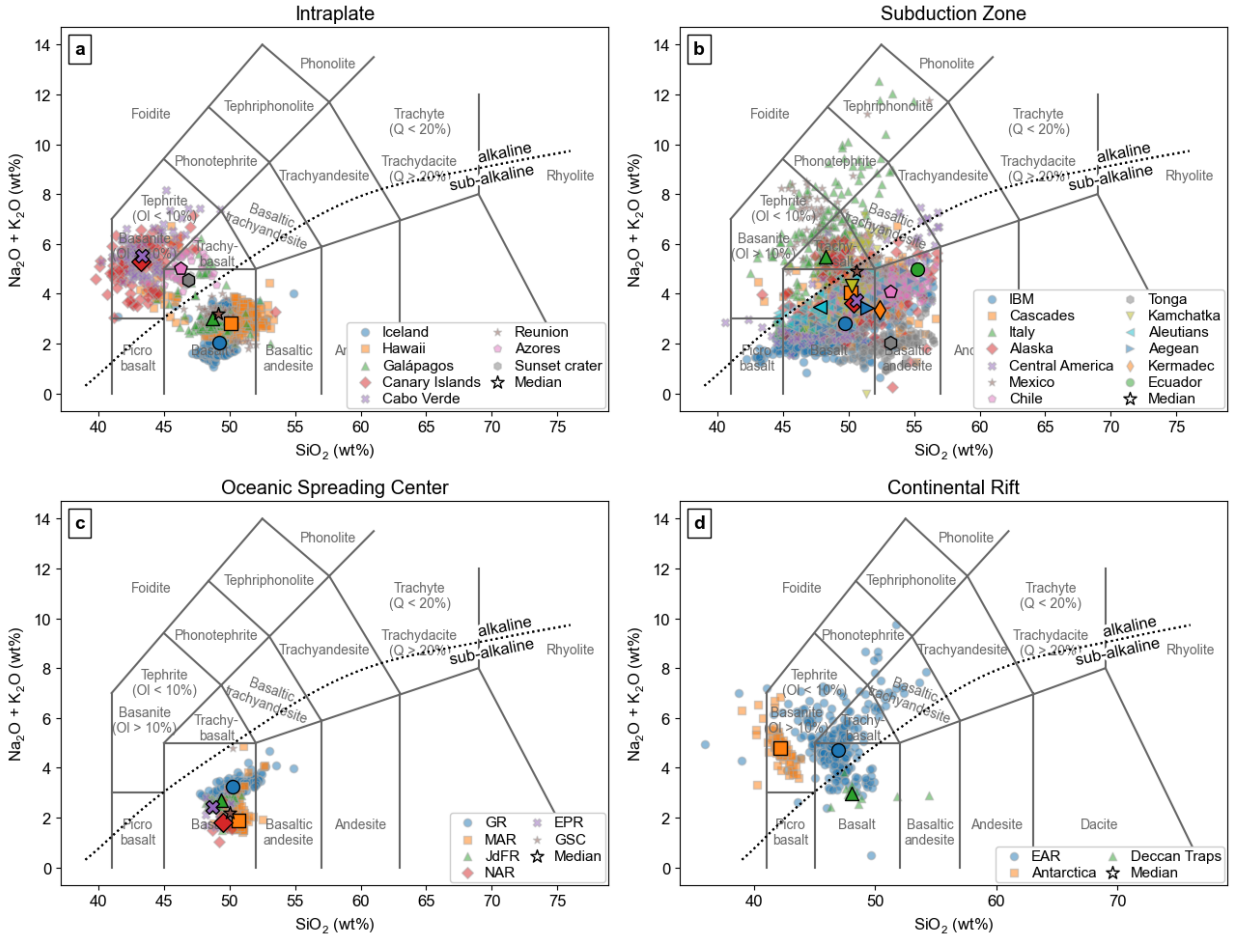

Figure S7. Total Alkalis vs Silica diagram for all the MI <57 wt% SiO_2 and MgO <16 wt% in our compilation. Larger black edged symbols indicate the medians of specific locations. (a) Intraplate (Oceanic and Continental) volcanoes in the compilation. We separate OIB-Tholeiitic and OIB-Alkaline locations based on the medians on this plot. (b) Subduction zone volcanoes. (c) Mid-Ocean Ridge (d) Continental Rifts.

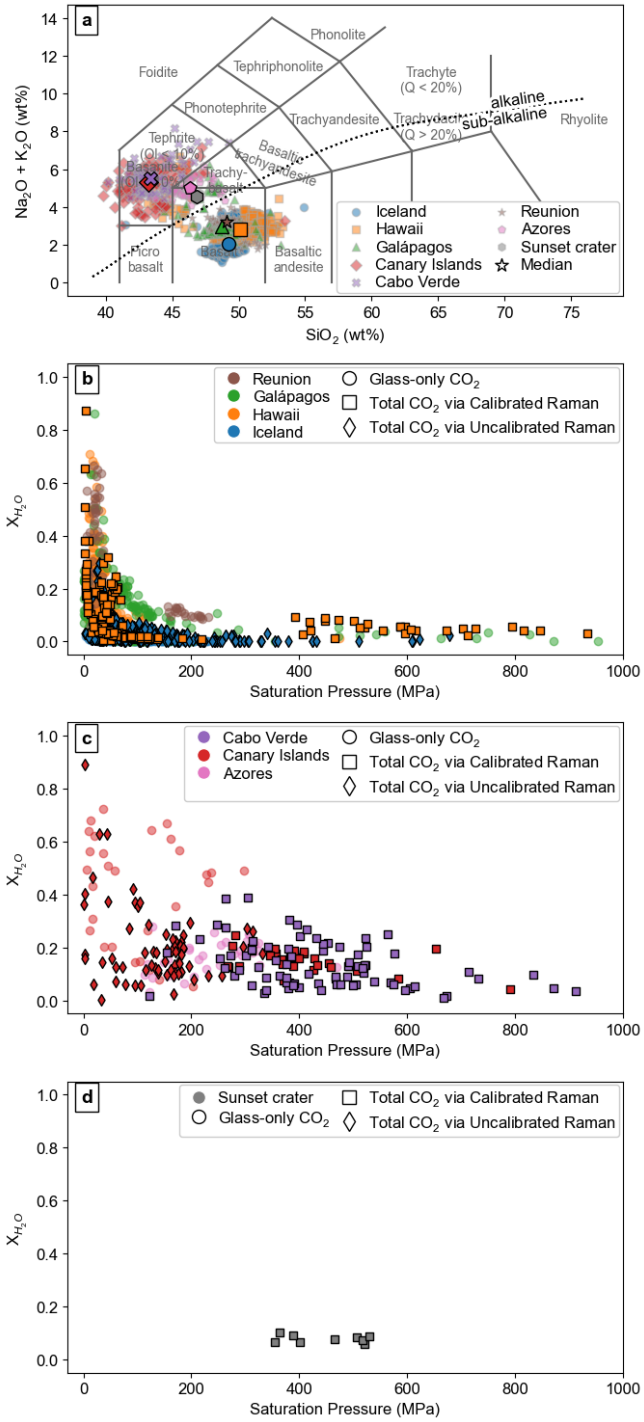

Figure S8. TAS diagram (a) and Pressure vs X_{H_2O} for Tholeiitic and Alkaline Ocean Island volcanoes and one continental intraplate volcano.

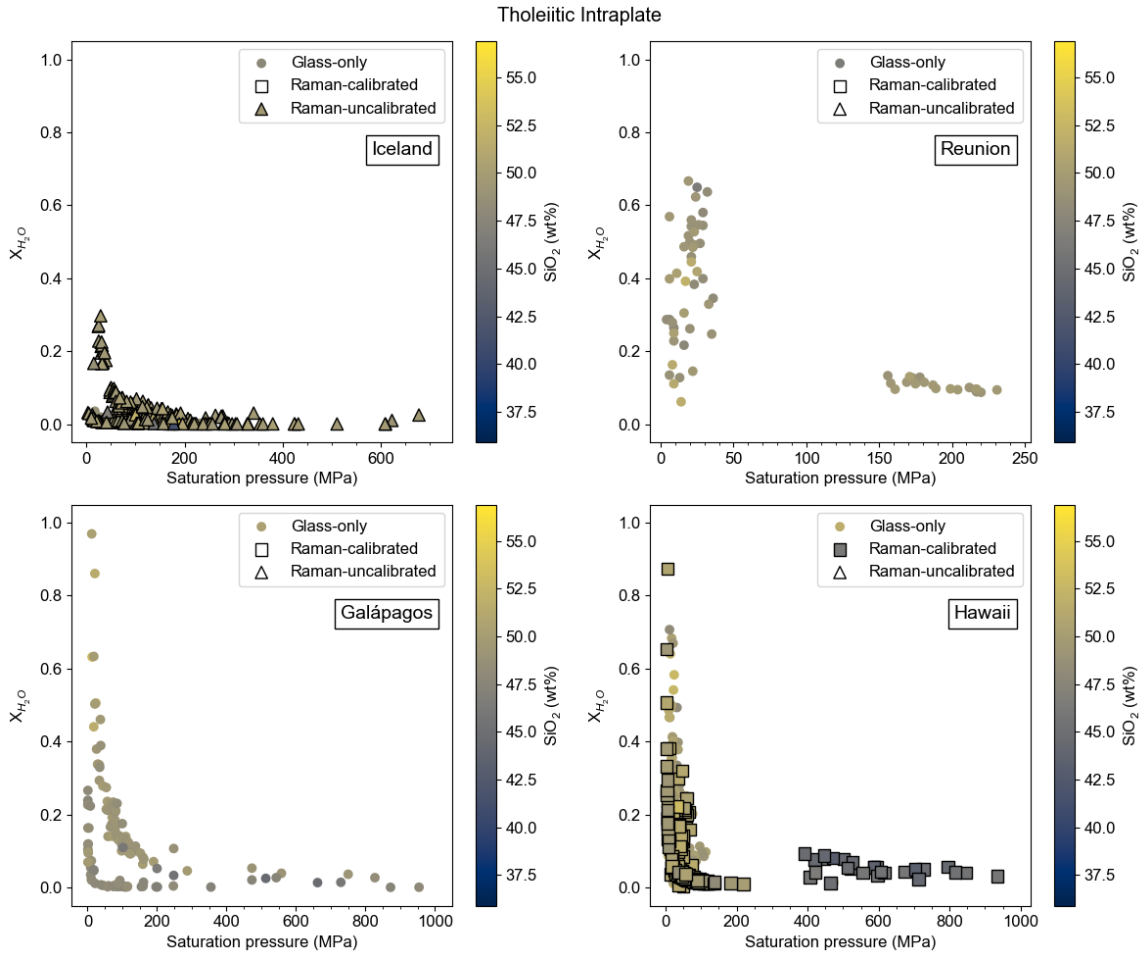

Figure S9a. Pressure vs X_{H_2O} at Tholeiitic OIB locations.

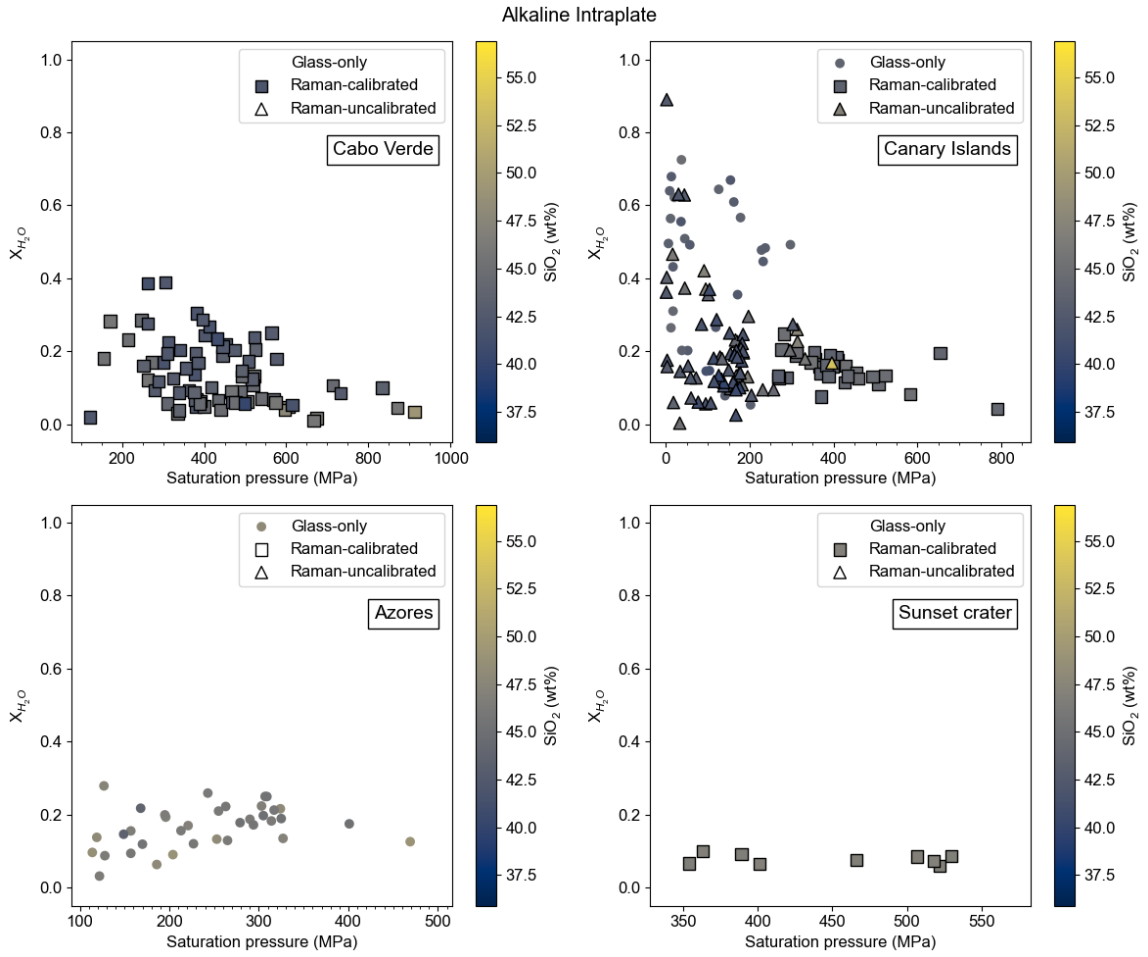

Figure S9b. Pressure vs X_{H_2O} at Alkaline OIB locations and sunset crater (an alkaline continental intraplate volcano).

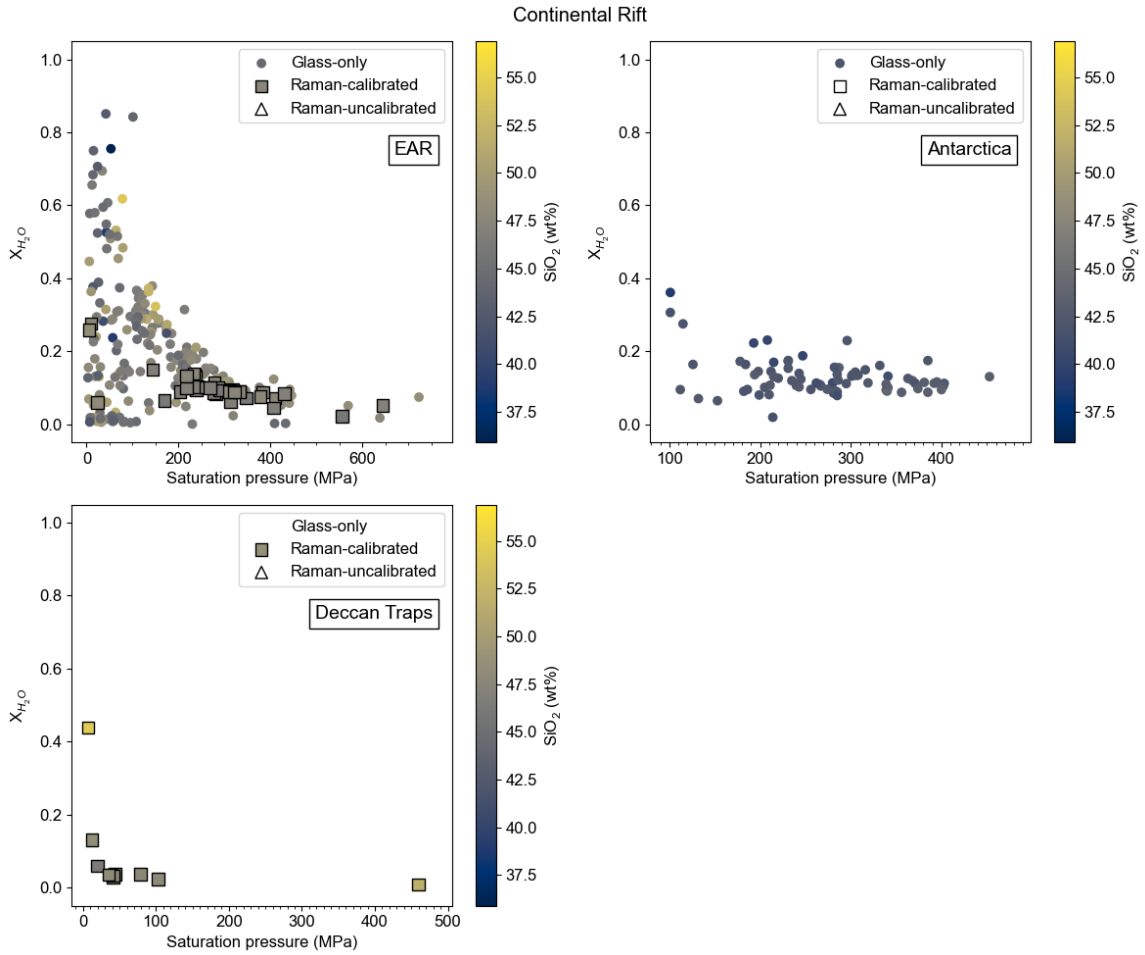

Figure S9c. Pressure vs X_{H_2O} at Continental rift locations.

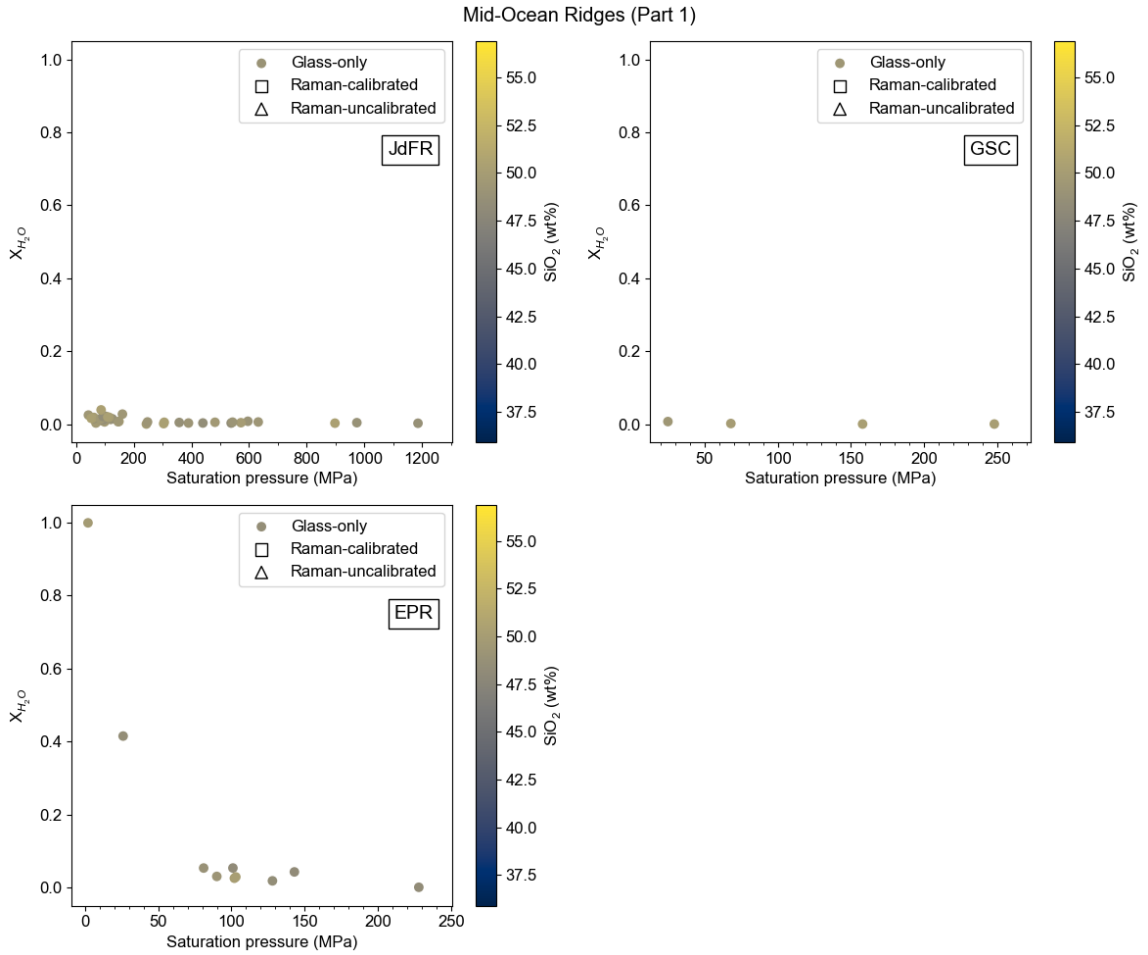

Figure S9d. Pressure vs X_{H_2O} at Mid-Ocean Ridge locations (Part 1). JdFR – Juan de Fuca Ridge, GSC – Galápagos Spreading Center, EPR – East Pacific Rise.

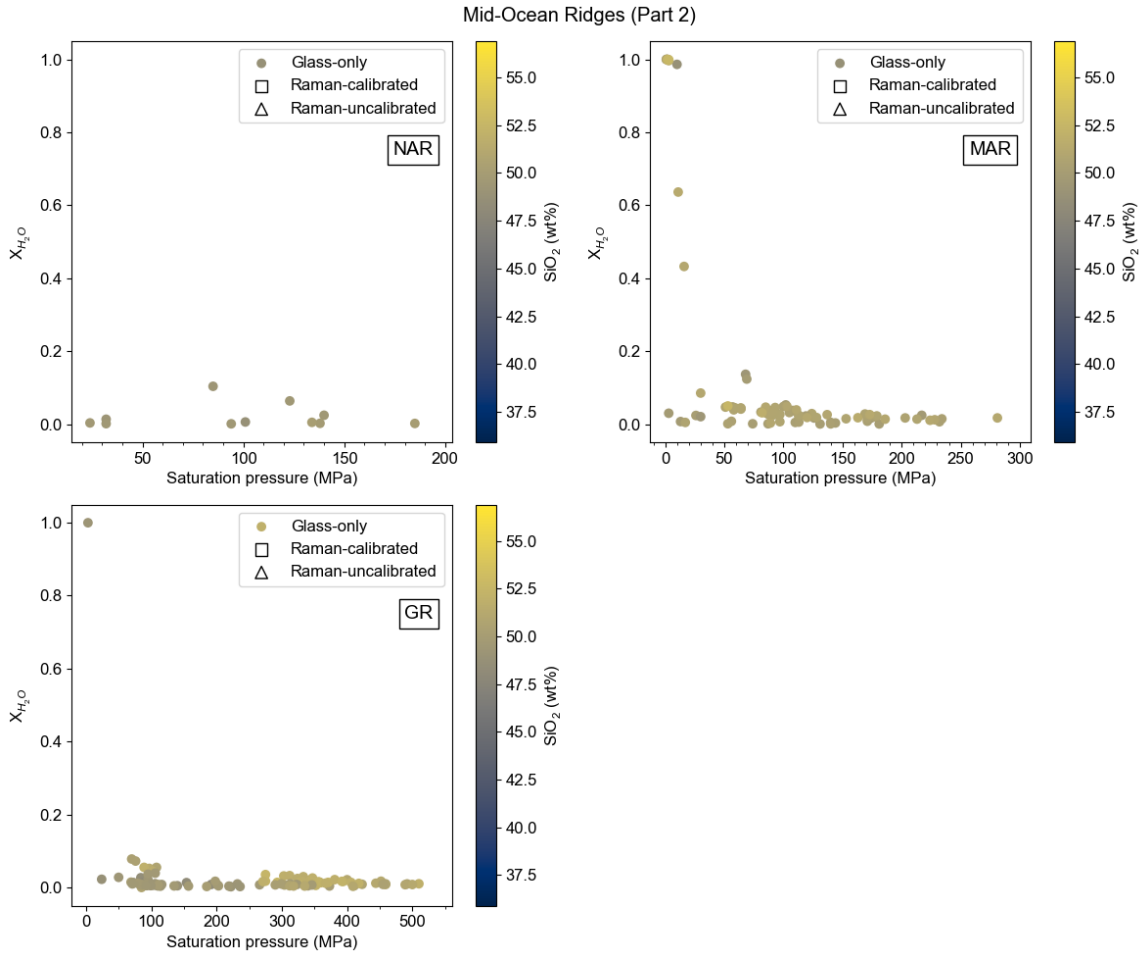

Figure S9e. Pressure vs X_{H_2O} at Mid-Ocean Ridge locations (Part 2). NAR – North Atlantic Ridge, MAR – Mid-Atlantic Ridge, GR – Gakkel Ridge.

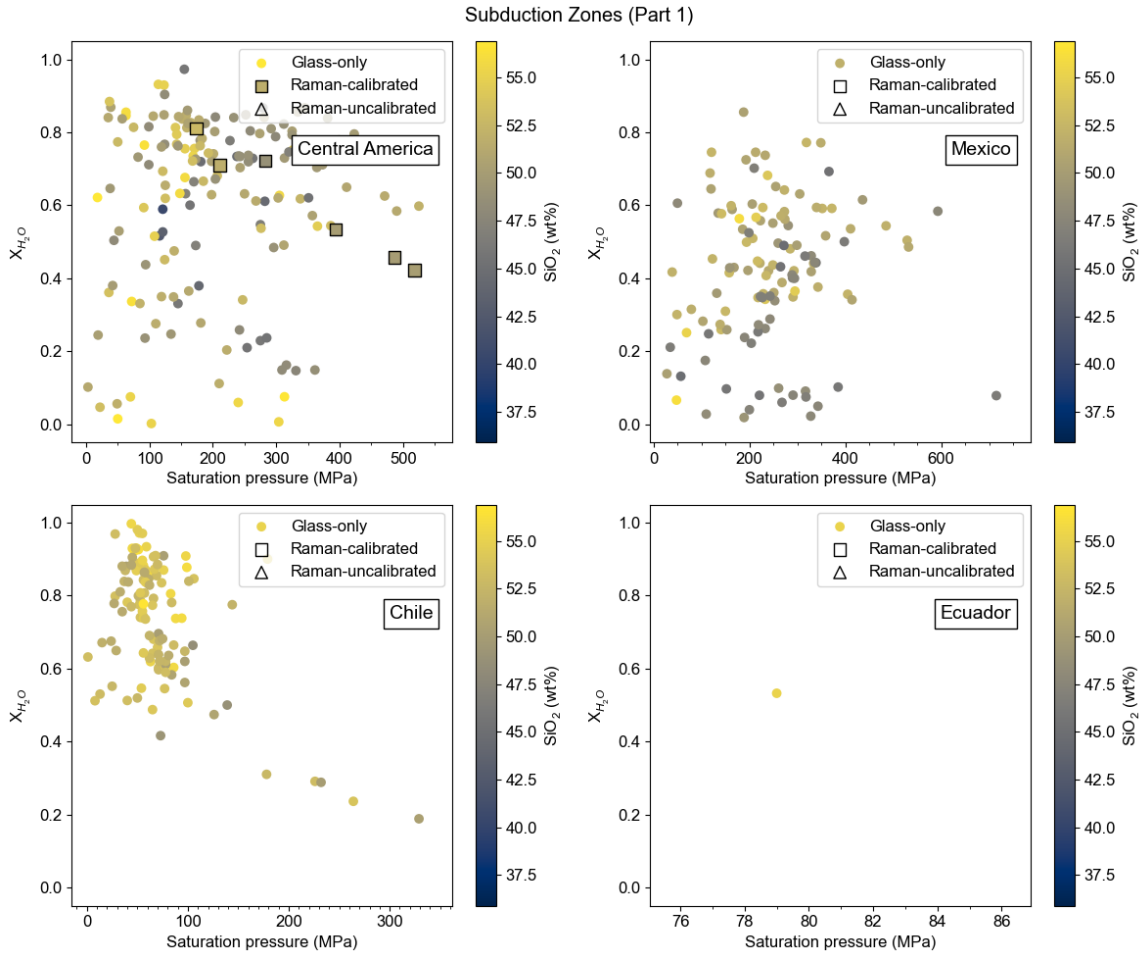

Figure S9f. Pressure vs X_{H_2O} at Subduction Zones (Part 1).

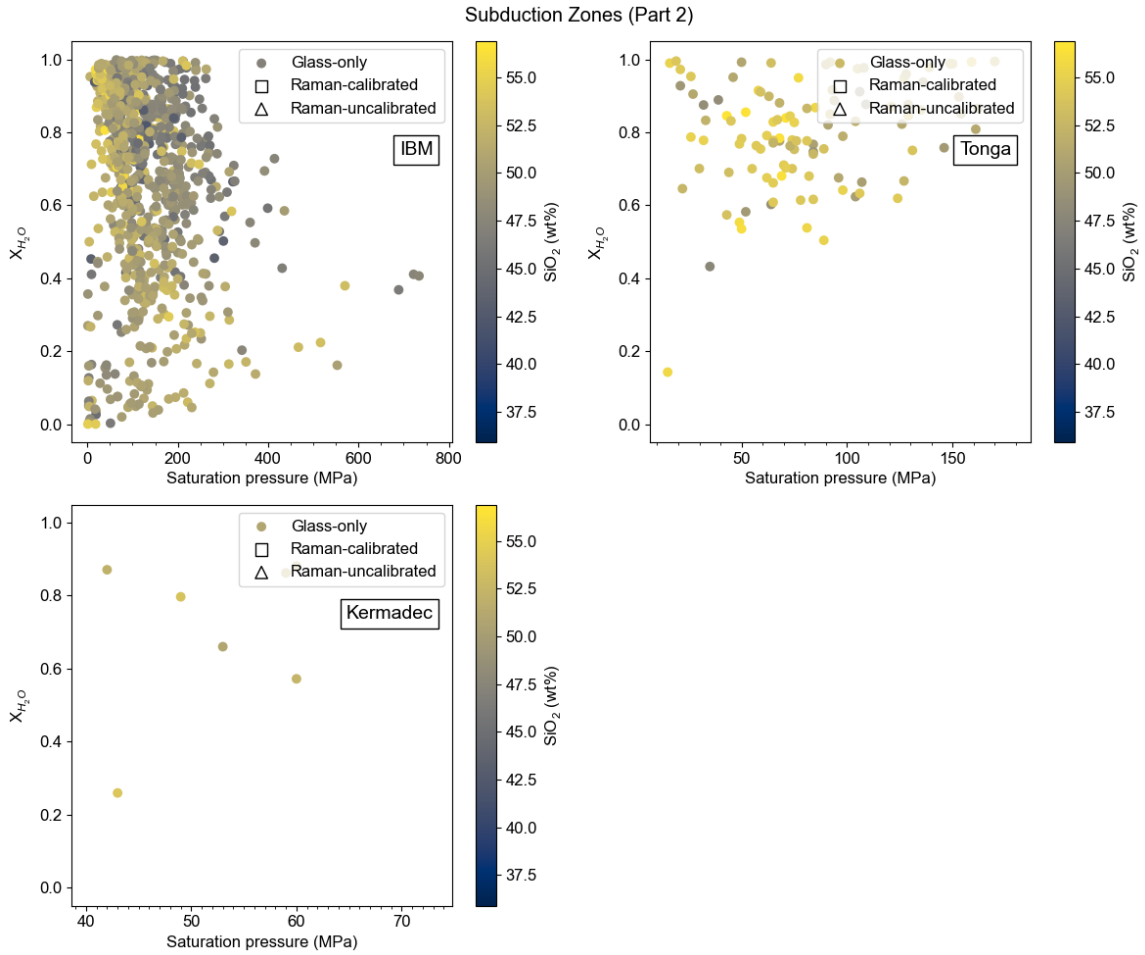

Figure S9g. Pressure vs X_{H_2O} at Subduction Zones (Part 2).

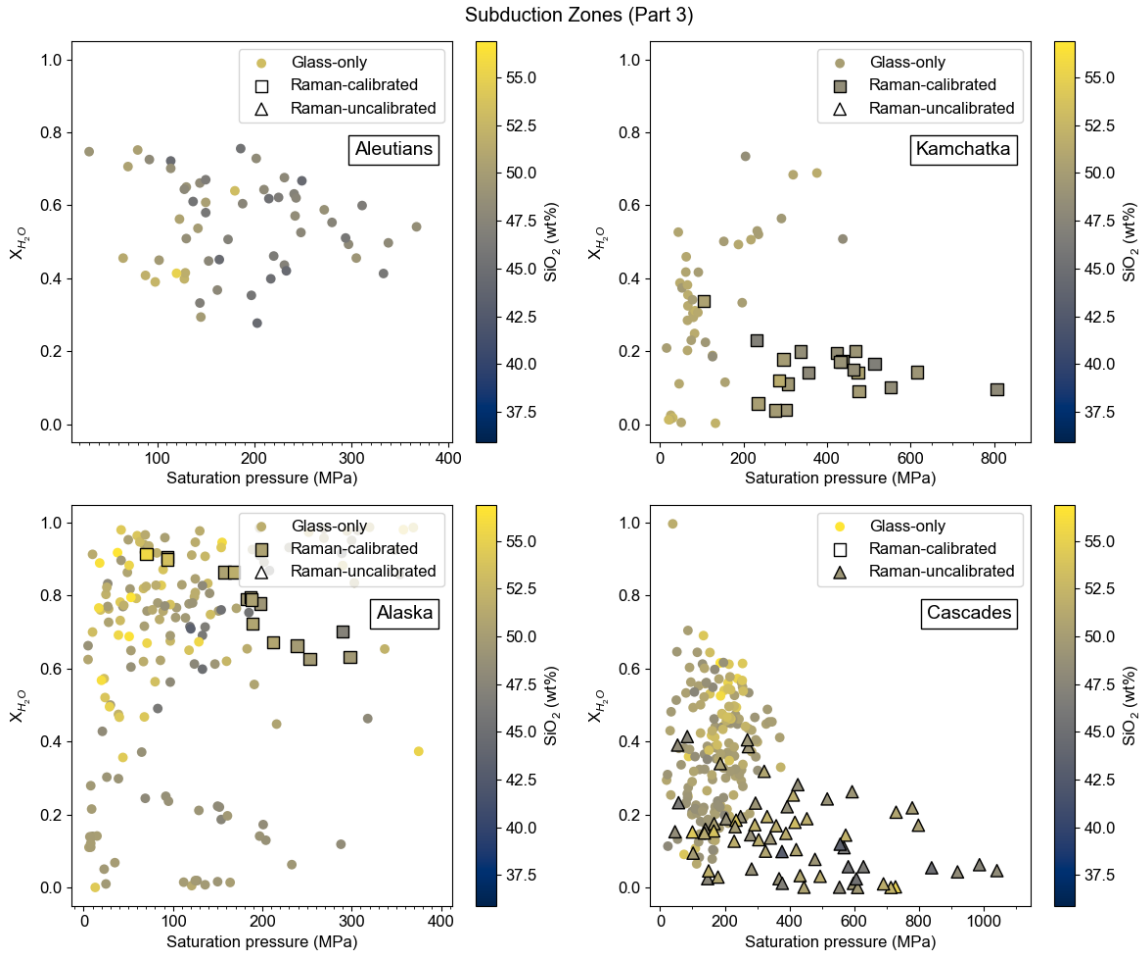

Figure S9h. Pressure vs X_{H_2O} at Subduction Zones (Part 3).

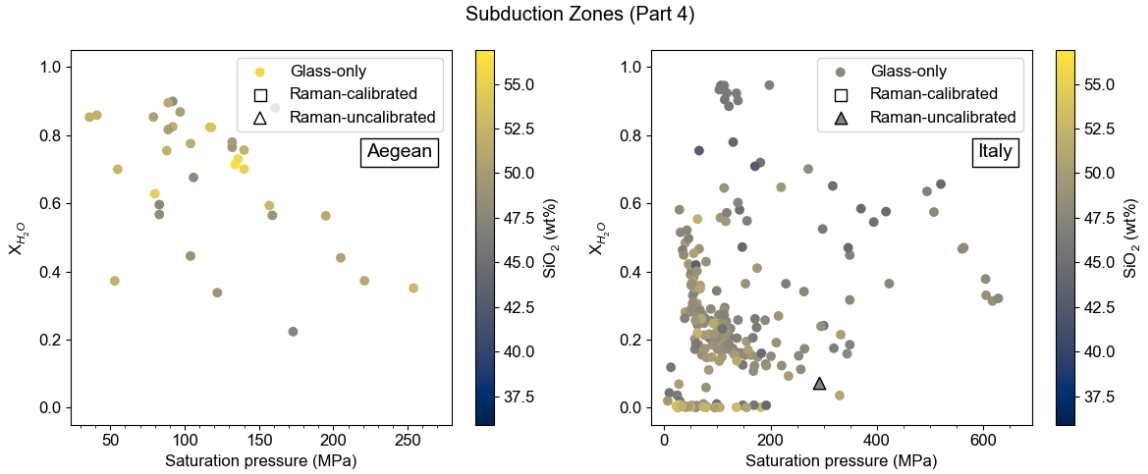

Figure S9i. Pressure vs X_{H_2O} at Subduction Zones (Part 4).

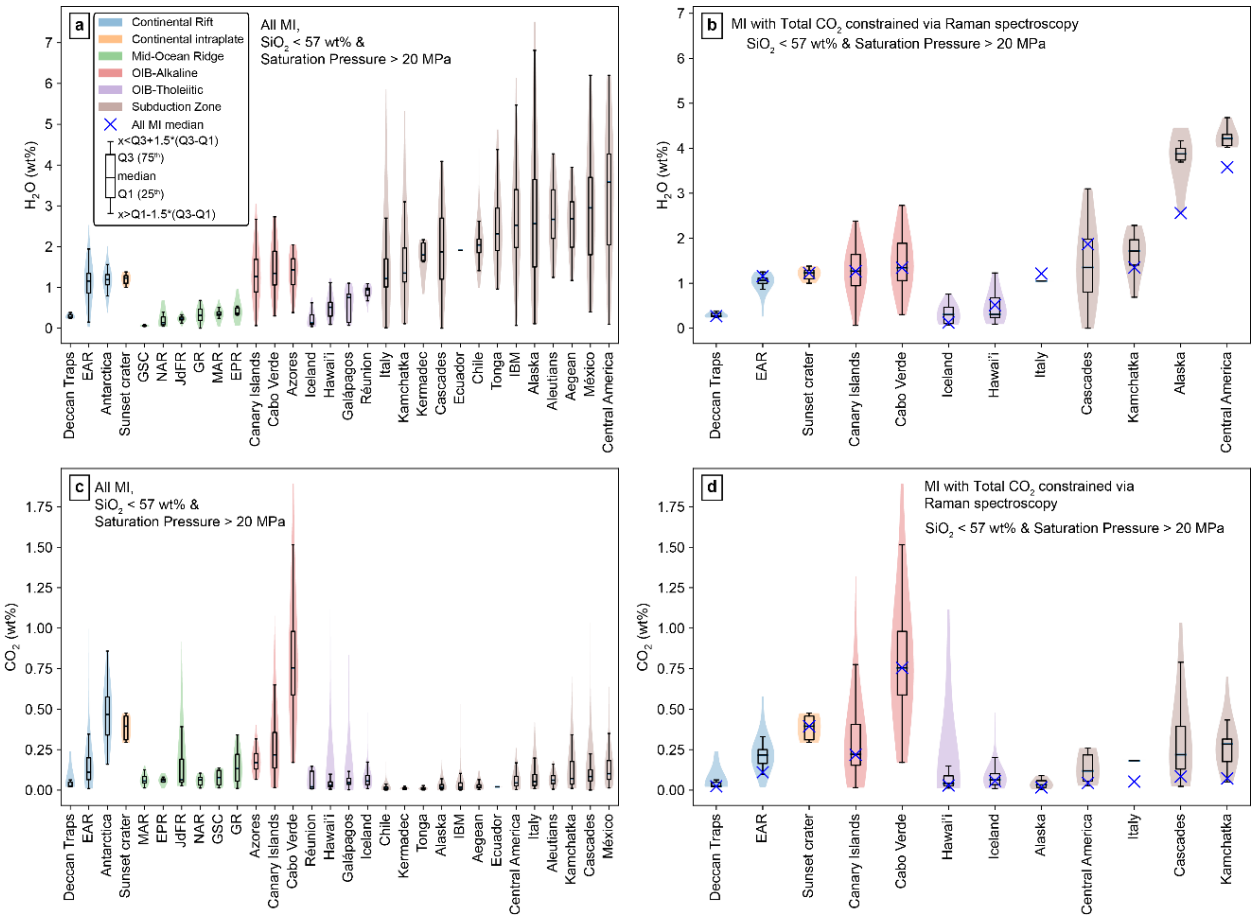

Figure S10. Boxplots and violin plots of H_2O and CO_2 contents of melt inclusions in the compilation. Filtered to SiO_2 < 57 wt%, MgO < 16 wt% and Saturation Pressure > 20MPa.

Data S2. (separate file)
Fluid inclusion dataset for this study.

Data S3. (separate file)
Global melt inclusion compilation (described in previous sections).

Supplementary references

1. C. L. DeVitre, P. E. Wieser, Reliability of Raman analyses of CO2-rich fluid inclusions as a geobarometer at Kīlauea. *Geochem. Perspect. Lett.* **29**, 1–8 (2024).

2. P. E. Wieser, C. L. DeVitre, DiadFit: An Open-SourcePython3 Tool for Peak fitting of Raman Data from silicate melts and CO2 fluids. EarthArXiv [Preprint] (2023). https://doi.org/10.31223/X5CQ1F.

3. R. Span, W. Wagner, A new equation of state for carbon dioxide covering the fluid region from the triple-point temperature to 1100 K at pressures up to 800 MPa. *J. Phys. Chem. Ref. Data* **25**, 1509–1596 (1996).

4. P. E. Wieser, H. Lamadrid, J. Maclennan, M. Edmonds, S. Matthews, K. Iacovino, F. E. Jenner, C. Gansecki, F. Trusdell, R. L. Lee, E. Ilyinskaya, Reconstructing Magma Storage Depths for the 2018 Kīlauean Eruption From Melt Inclusion CO2 Contents: The Importance of Vapor Bubbles. *Geochem. Geophys. Geosystems* **22**, e2020GC009364 (2021).

5. A. H. Lerner, P. J. Wallace, T. Shea, A. J. Mourey, P. J. Kelly, P. A. Nadeau, T. Elias, C. Kern, L. E. Clor, C. Gansecki, The petrologic and degassing behavior of sulfur and other magmatic volatiles from the 2018 eruption of Kīlauea, Hawai‘i: melt concentrations, magma storage depths, and magma recycling. *Bull. Volcanol.* **83**, 1–32 (2021).

6. M. P. Ryan, The elasticity and contractancy of Hawaiian olivine tholeiite, and its role in the stability and structural evolution of sub-caldera magma reservoirs and rift systems. In Volcanism in Hawaii. *US Geol Surv Prof Pap* **1350**, 1395–1447 (1987).

7. E. Jarosewich, J. A. Nelen, J. A. Norberg, Reference samples for electron microprobe analysis. *Geostand. Newsl.* **4**, 43–47 (1980).

8. P. E. Wieser, A. J. R. Kent, C. B. Till, J. Donovan, D. A. Neave, D. L. Blatter, M. J. Krawczynski, Barometers Behaving Badly I: Assessing the Influence of Analytical and Experimental Uncertainty on Clinopyroxene Thermobarometry Calculations at Crustal Conditions. *J. Petrol.* **64**, egac126 (2023).

9. J. T. Armstrong, Accurate quantitative analysis of oxygen and nitrogen with a W/Si multilayer crystal. *Microbeam Anal.*, 301–304 (1988).

10. C. Gansecki, R. L. Lee, T. Shea, S. P. Lundblad, K. Hon, C. Parcheta, The tangled tale of Kīlauea's 2018 eruption as told by geochemical monitoring. *Science* **366**, eaaz0147 (2019).

11. T. H. Hansteen, A. Klügel, Fluid Inclusion Thermobarometry as a Tracer for Magmatic Processes. *Rev. Mineral. Geochem.* **69**, 143–177 (2008).

12. S. Yoshimura, Carbon dioxide and water in the crust. Part 1: Equation of state for the fluid. *J. Mineral. Petrol. Sci.* **118**, 221224a (2023).

13. S. M. Sterner, K. S. Pitzer, An equation of state for carbon dioxide valid from zero to extreme pressures. *Contrib. Mineral. Petrol.* **117**, 362–374 (1994).

14. Z. Duan, Z. Zhang, Equation of state of the H2O, CO2, and H2O–CO2 systems up to 10 GPa and 2573.15K: Molecular dynamics simulations with ab initio potential surface. *Geochim. Cosmochim. Acta* **70**, 2311–2324 (2006).

15. A. H. Lerner, D. M. Sublett, P. J. Wallace, C. Cauley, R. J. Bodnar, Insights into magma storage depths and eruption controls at Kīlauea Volcano during explosive and effusive periods of the past 500 years based on melt and fluid inclusions. *Earth Planet. Sci. Lett.* **628**, 118579 (2024).

16. D. J. Rasmussen, T. Plank, E. Cottrell, A. Johansson, K. Lehnert, E. Hauri, DCO-EarthChem Melt Inclusion Expert Dataset, EARTHCHEM (2022); https://doi.org/10.26022/IEDA/112364.

17. C. L. DeVitre, E. Gazel, R. S. Ramalho, S. Venugopal, M. Steele-MacInnis, J. Hua, C. M. Allison, L. R. Moore, J. C. Carracedo, B. Monteleone, Oceanic intraplate explosive eruptions fed directly from the mantle. *Proc. Natl. Acad. Sci.* **120**, e2302093120 (2023).

18. P. E. Wieser, A. Kent, C. Till, G. Abers, Geophysical and Geochemical Constraints on Magma Storage Depths along the Cascade Arc: Knowns and Unknowns. EarthArXiv [Preprint] (2023). https://doi.org/10.31223/X5KX00.

19. D. M. Harris, A. T. Anderson Jr, Concentrations, sources, and losses of H2O, CO2, and S in Kilauean basalt. *Geochim. Cosmochim. Acta* **47**, 1139–1150 (1983).

20. A. T. Anderson, G. G. Brown, CO2 contents and formation pressures of some Kilauean melt inclusions. *Am. Mineral.* **78**, 794–803 (1993).

21. K. Roggensack, R. L. Hervig, S. B. McKnight, S. N. Williams, Explosive basaltic volcanism from Cerro Negro volcano: influence of volatiles on eruptive style. *Science* **277**, 1639–1642 (1997).

22. K. Roggensack, Unraveling the 1974 eruption of Fuego volcano (Guatemala) with small crystals and their young melt inclusions. *Geology* **29**, 911–914 (2001).

23. K. Roggensack, Sizing up crystals and their melt inclusions: a new approach to crystallization studies. *Earth Planet. Sci. Lett.* **187**, 221–237 (2001).

24. A. E. Saal, E. H. Hauri, C. H. Langmuir, M. R. Perfit, Vapour undersaturation in primitive mid-ocean-ridge basalt and the volatile content of Earth's upper mantle. *Nature* **419**, 451–455 (2002).

25. P. Cervantes, P. Wallace, Magma degassing and basaltic eruption styles: a case study of ~2000 year BP Xitle volcano in central Mexico. *J. Volcanol. Geotherm. Res.* **120**, 249–270 (2003).

26. J. A. Wade, T. Plank, W. G. Melson, G. J. Soto, E. H. Hauri, The volatile content of magmas from Arenal volcano, Costa Rica. *J. Volcanol. Geotherm. Res.* **157**, 94–120 (2006).

27. E. R. Benjamin, T. Plank, J. A. Wade, K. A. Kelley, E. H. Hauri, G. E. Alvarado, High water contents in basaltic magmas from Irazú Volcano, Costa Rica. *J. Volcanol. Geotherm. Res.* **168**, 68–92 (2007).

28. S. J. Sadofsky, M. Portnyagin, K. Hoernle, P. van den Bogaard, Subduction cycling of volatiles and trace elements through the Central American volcanic arc: evidence from melt inclusions. *Contrib. Mineral. Petrol.* **155**, 433–456 (2008).

29. N. Vigouroux, P. J. Wallace, A. J. R. Kent, Volatiles in High-K Magmas from the Western Trans-Mexican Volcanic Belt: Evidence for Fluid Fluxing and Extreme Enrichment of the Mantle Wedge by Subduction Processes. *J. Petrol.* **49**, 1589–1618 (2008).

30. S. Auer, I. Bindeman, P. Wallace, V. Ponomareva, M. Portnyagin, The origin of hydrous, high-δ18O voluminous volcanism: diverse oxygen isotope values and high magmatic water contents within the volcanic record of Klyuchevskoy volcano, Kamchatka, Russia. *Contrib. Mineral. Petrol.* **157**, 209–230 (2009).

31. V. Famin, B. Welsch, S. Okumura, P. Bachèlery, S. Nakashima, Three differentiation stages of a single magma at Piton de la Fournaise volcano (Reunion hot spot). *Geochem. Geophys. Geosystems* **10** (2009).

32. E. R. Johnson, P. J. Wallace, H. Delgado Granados, V. C. Manea, A. J. R. Kent, I. N. Bindeman, C. S. Donegan, Subduction-related Volatile Recycling and Magma Generation beneath Central Mexico: Insights from Melt Inclusions, Oxygen Isotopes and Geodynamic Models. *J. Petrol.* **50**, 1729–1764 (2009).

33. K. A. Kelley, E. Cottrell, Water and the Oxidation State of Subduction Zone Magmas. *Science* **325**, 605–607 (2009).

34. A. M. Koleszar, A. E. Saal, E. H. Hauri, A. N. Nagle, Y. Liang, M. D. Kurz, The volatile contents of the Galapagos plume; evidence for H2O and F open system behavior in melt inclusions. *Earth Planet. Sci. Lett.* **287**, 442–452 (2009).

35. J. Roberge, H. Delgado-Granados, P. J. Wallace, Mafic magma recharge supplies high CO2 and SO2 gas fluxes from Popocatépetl volcano, Mexico. *Geology* **37**, 107–110 (2009).

36. M. M. Zimmer, *Water in Aleutian Magmas: Its Origins in the Subduction Zone and Its Effects on Magma Evolution* (ProQuest, 2009).

37. L. B. Cooper, T. Plank, R. J. Arculus, E. H. Hauri, P. S. Hall, S. W. Parman, High-Ca boninites from the active Tonga Arc. *J. Geophys. Res. Solid Earth* **115** (2010).

38. L. Cooper, T. Plank, R. Arculus, E. Hauri, K. A. Kelley, Arc–Backarc Exchange Along the Tonga–Lau System: Constraints From Volatile Elements. *J. Petrol.* **63**, egac072 (2022).

39. K. A. Kelley, T. Plank, S. Newman, E. M. Stolper, T. L. Grove, S. Parman, E. H. Hauri, Mantle Melting as a Function of Water Content beneath the Mariana Arc. *J. Petrol.* **51**, 1711–1738 (2010).

40. D. M. Ruscitto, P. J. Wallace, E. R. Johnson, A. J. R. Kent, I. N. Bindeman, Volatile contents of mafic magmas from cinder cones in the Central Oregon High Cascades: Implications for magma formation and mantle conditions in a hot arc. *Earth Planet. Sci. Lett.* **298**, 153–161 (2010).

41. D. M. Ruscitto, P. J. Wallace, A. J. R. Kent, Revisiting the compositions and volatile contents of olivine-hosted melt inclusions from the Mount Shasta region: implications for the formation of high-Mg andesites. *Contrib. Mineral. Petrol.* **162**, 109–132 (2011).

42. A. M. Shaw, M. D. Behn, S. E. Humphris, R. A. Sohn, P. M. Gregg, Deep pooling of low degree melts and volatile fluxes at the 85°E segment of the Gakkel Ridge: Evidence from olivine-hosted melt inclusions and glasses. *Earth Planet. Sci. Lett.* **289**, 311–322 (2010).

43. M. M. Zimmer, T. Plank, E. H. Hauri, G. M. Yogodzinski, P. Stelling, J. Larsen, B. Singer, B. Jicha, C. Mandeville, C. J. Nye, The Role of Water in Generating the Calc-alkaline Trend: New Volatile Data for Aleutian Magmas and a New Tholeiitic Index. *J. Petrol.* **51**, 2411–2444 (2010).

44. R. Esposito, R. J. Bodnar, L. V. Danyushevsky, B. De Vivo, L. Fedele, J. Hunter, A. Lima, N. Shimizu, Volatile Evolution of Magma Associated with the Solchiaro Eruption in the Phlegrean Volcanic District (Italy). *J. Petrol.* **52**, 2431–2460 (2011).

45. E. M. Head, A. M. Shaw, P. J. Wallace, K. W. W. Sims, S. A. Carn, Insight into volatile behavior at Nyamuragira volcano (D.R. Congo, Africa) through olivine-hosted melt inclusions. *Geochem. Geophys. Geosystems* **12** (2011).

46. C. Helo, M.-A. Longpré, N. Shimizu, D. A. Clague, J. Stix, Explosive eruptions at mid-ocean ridges driven by CO2-rich magmas. *Nat. Geosci.* **4**, 260–263 (2011).

47. A. Mormone, M. Piochi, F. Bellatreccia, G. De Astis, R. Moretti, G. D. Ventura, A. Cavallo, A. Mangiacapra, A CO2-rich magma source beneath the Phlegraean Volcanic District (Southern Italy): Evidence from a melt inclusion study. *Chem. Geol.* **287**, 66–80 (2011).

48. C. I. Schipper, J. D. L. White, B. F. Houghton, Textural, geochemical, and volatile evidence for a Strombolian-like eruption sequence at Lō`ihi Seamount, Hawai`i. *J. Volcanol. Geotherm. Res.* **207**, 16–32 (2011).

49. K. Berlo, J. Stix, K. Roggensack, B. Ghaleb, A tale of two magmas, Fuego, Guatemala. *Bull. Volcanol.* **74**, 377–390 (2012).

50. C. Bouvet de Maisonneuve, M. A. Dungan, O. Bachmann, A. Burgisser, Insights into shallow magma storage and crystallization at Volcán Llaima (Andean Southern Volcanic Zone, Chile). *J. Volcanol. Geotherm. Res.* **211–212**, 76–91 (2012).

51. L. Field, J. Blundy, R. A. Brooker, T. Wright, G. Yirgu, Magma storage conditions beneath Dabbahu Volcano (Ethiopia) constrained by petrology, seismicity and satellite geodesy. *Bull. Volcanol.* **74**, 981–1004 (2012).

52. E. F. Rose-Koga, K. T. Koga, P. Schiano, M. Le Voyer, N. Shimizu, M. J. Whitehouse, R. Clocchiatti, Mantle source heterogeneity for South Tyrrhenian magmas revealed by Pb isotopes and halogen contents of olivine-hosted melt inclusions. *Chem. Geol.* **334**, 266–279 (2012).

53. V. D. Wanless, A. M. Shaw, Lower crustal crystallization and melt evolution at mid-ocean ridges. *Nat. Geosci.* **5**, 651–655 (2012).

54. R. J. Wysoczanski, M. R. Handler, C. I. Schipper, M. I. Leybourne, J. Creech, M. D. Rotella, A. R. L. Nichols, C. J. N. Wilson, R. B. Stewart, The Tectonomagmatic Source of Ore Metals and Volatile Elements in the Southern Kermadec Arc. *Econ. Geol.* **107**, 1539–1556 (2012).

55. J. M. de Moor, T. P. Fischer, P. L. King, R. E. Botcharnikov, R. L. Hervig, D. R. Hilton, P. H. Barry, F. Mangasini, C. Ramirez, Volatile-rich silicate melts from Oldoinyo Lengai volcano (Tanzania): Implications for carbonatite genesis and eruptive behavior. *Earth Planet. Sci. Lett.* **361**, 379–390 (2013).

56. A. S. Lloyd, T. Plank, P. Ruprecht, E. H. Hauri, W. Rose, Volatile loss from melt inclusions in pyroclasts of differing sizes. *Contrib. Mineral. Petrol.* **165**, 129–153 (2013).

57. M. N. Brounce, K. A. Kelley, E. Cottrell, Variations in Fe3+/∑Fe of Mariana Arc Basalts and Mantle Wedge fO2. *J. Petrol.* **55**, 2513–2536 (2014).

58. M. E. Hartley, J. Maclennan, M. Edmonds, T. Thordarson, Reconstructing the deep CO2 degassing behaviour of large basaltic fissure eruptions. *Earth Planet. Sci. Lett.* **393**, 120–131 (2014).

59. N. Métrich, V. Zanon, L. Créon, A. Hildenbrand, M. Moreira, F. O. Marques, Is the 'Azores Hotspot' a Wetspot? Insights from the Geochemistry of Fluid and Melt Inclusions in Olivine of Pico Basalts. *J. Petrol.* **55**, 377–393 (2014).

60. M. L. Myers, D. J. Geist, M. C. Rowe, K. S. Harpp, P. J. Wallace, J. Dufek, Replenishment of volatile-rich mafic magma into a degassed chamber drives mixing and eruption of Tungurahua volcano. *Bull. Volcanol.* **76**, 872 (2014).

61. I. Sides, M. Edmonds, J. Maclennan, B. F. Houghton, D. A. Swanson, M. J. Steele-MacInnis, Magma mixing and high fountaining during the 1959 Kīlauea Iki eruption, Hawai 'i. *Earth Planet. Sci. Lett.* **400**, 102–112 (2014).

62. V. D. Wanless, M. D. Behn, A. M. Shaw, T. Plank, Variations in melting dynamics and mantle compositions along the Eastern Volcanic Zone of the Gakkel Ridge: insights from olivine-hosted melt inclusions. *Contrib. Mineral. Petrol.* **167**, 1005 (2014).

63. V. D. Wanless, A. M. Shaw, M. D. Behn, S. A. Soule, J. Escartín, C. Hamelin, Magmatic plumbing at Lucky Strike volcano based on olivine-hosted melt inclusion compositions. *Geochem. Geophys. Geosystems* **16**, 126–147 (2015).

64. M. Cassidy, M. Edmonds, S. F. L. Watt, M. R. Palmer, T. M. Gernon, Origin of Basalts by Hybridization in Andesite-dominated Arcs. *J. Petrol.* **56**, 325–346 (2015).

65. A. Colman, J. M. Sinton, V. D. Wanless, Constraints from melt inclusions on depths of magma residence at intermediate magma supply along the Galápagos Spreading Center. *Earth Planet. Sci. Lett.* **412**, 122–131 (2015).

66. T. R. Hudgins, S. B. Mukasa, A. C. Simon, G. Moore, E. Barifaijo, Melt inclusion evidence for CO2-rich melts beneath the western branch of the East African Rift: implications for long-term storage of volatiles in the deep lithospheric mantle. *Contrib. Mineral. Petrol.* **169**, 46 (2015).

67. L. R. Moore, E. Gazel, R. Tuohy, A. S. Lloyd, R. Esposito, M. Steele-MacInnis, E. H. Hauri, P. J. Wallace, T. Plank, R. J. Bodnar, Bubbles matter: An assessment of the contribution of vapor bubbles to melt inclusion volatile budgets. *Am. Mineral.* **100**, 806–823 (2015).

68. L. R. Moore, N. Mironov, M. Portnyagin, E. Gazel, R. J. Bodnar, Volatile contents of primitive bubble-bearing melt inclusions from Klyuchevskoy volcano, Kamchatka: Comparison of volatile contents determined by mass-balance versus experimental homogenization. *J. Volcanol. Geotherm. Res.* **358**, 124–131 (2018).

69. L. R. Moore, E. Gazel, R. J. Bodnar, The volatile budget of Hawaiian magmatism: Constraints from melt inclusions from Haleakala volcano, Hawaii. *J. Volcanol. Geotherm. Res.* **410**, 107144 (2021).

70. P. Plechov, J. Blundy, N. Nekrylov, E. Melekhova, V. Shcherbakov, M. S. Tikhonova, Petrology and volatile content of magmas erupted from Tolbachik Volcano, Kamchatka, 2012–13. *J. Volcanol. Geotherm. Res.* **307**, 182–199 (2015).

71. J. M. Ribeiro, R. J. Stern, K. A. Kelley, A. M. Shaw, F. Martinez, Y. Ohara, Composition of the slab-derived fluids released beneath the Mariana forearc: Evidence for shallow dehydration of the subducting plate. *Earth Planet. Sci. Lett.* **418**, 136–148 (2015).

72. P. J. Wallace, V. S. Kamenetsky, P. Cervantes, Melt inclusion CO2 contents, pressures of olivine crystallization, and the problem of shrinkage bubbles. *Am. Mineral.* **100**, 787–794 (2015).

73. E. M. Aster, P. J. Wallace, L. R. Moore, J. Watkins, E. Gazel, R. J. Bodnar, Reconstructing CO2 concentrations in basaltic melt inclusions using Raman analysis of vapor bubbles. *J. Volcanol. Geotherm. Res.* **323**, 148–162 (2016).

74. T. H. Druitt, M. Mercier, L. Florentin, E. Deloule, N. Cluzel, T. Flaherty, E. Médard, A. Cadoux, Magma Storage and Extraction Associated with Plinian and Interplinian Activity at Santorini Caldera (Greece). *J. Petrol.* **57**, 461–494 (2016).

75. D. C. S. Ruth, E. Cottrell, J. A. Cortés, K. A. Kelley, E. S. Calder, From Passive Degassing to Violent Strombolian Eruption: the Case of the 2008 Eruption of Llaima Volcano, Chile. *J. Petrol.* **57**, 1833–1864 (2016).

76. S. Venugopal, S. Moune, G. Williams-Jones, Investigating the subsurface connection beneath Cerro Negro volcano and the El Hoyo Complex, Nicaragua. *J. Volcanol. Geotherm. Res.* **325**, 211–224 (2016).

77. S. Venugopal, S. Moune, G. Williams-Jones, T. Druitt, N. Vigouroux, A. Wilson, J. K. Russell, Two distinct mantle sources beneath the Garibaldi Volcanic Belt: Insight from olivine-hosted melt inclusions. *Chem. Geol.* **532**, 119346 (2020).

78. S. Venugopal, S. Moune, G. Williams-Jones, T. Druitt, N. Vigouroux, A. Wilson, J. K. Russell, Two distinct mantle sources beneath the Garibaldi Volcanic Belt: Insight from olivine-hosted melt inclusions. *Chem. Geol.* **532**, 119346 (2020).

79. K. J. Walowski, P. J. Wallace, M. A. Clynne, D. J. Rasmussen, D. Weis, Slab melting and magma formation beneath the southern Cascade arc. *Earth Planet. Sci. Lett.* **446**, 100–112 (2016).

80. K. J. Walowski, L. A. Kirstein, J. C. M. De Hoog, T. R. Elliott, I. P. Savov, R. E. Jones, Investigating ocean island mantle source heterogeneity with boron isotopes in melt inclusions. *Earth Planet. Sci. Lett.* **508**, 97–108 (2019).

81. A. Donovan, J. Blundy, C. Oppenheimer, I. Buisman, The 2011 eruption of Nabro volcano, Eritrea: perspectives on magmatic processes from melt inclusions. *Contrib. Mineral. Petrol.* **173**, 1 (2017).

82. E. H. Hauri, J. Maclennan, D. McKenzie, K. Gronvold, N. Oskarsson, N. Shimizu, CO2 content beneath northern Iceland and the variability of mantle carbon. *Geology* **46**, 55–58 (2017).

83. E. Hauri, T. Plank, T. P. Fischer, Y. Tamura, O. Ishizuka, Melt Inclusion data from the Marianas and Izu volcanic arcs, and Mariana Trough back-arc basin, EARTHCHEM (2021); https://doi.org/doi.org/10.1016/j.epsl.2008.08.015.

84. M.-A. Longpré, J. Stix, A. Klügel, N. Shimizu, Mantle to surface degassing of carbon- and sulphur-rich alkaline magma at El Hierro, Canary Islands. *Earth Planet. Sci. Lett.* **460**, 268–280 (2017).

85. D. J. Rasmussen, P. R. Kyle, P. J. Wallace, K. W. W. Sims, G. A. Gaetani, E. H. Phillips, Understanding Degassing and Transport of CO2-rich Alkalic Magmas at Ross Island, Antarctica using Olivine-Hosted Melt Inclusions. *J. Petrol.* **58**, 841–861 (2017).

86. P. Robidoux, S. G. Rotolo, A. Aiuppa, G. Lanzo, E. H. Hauri, Geochemistry and volatile content of magmas feeding explosive eruptions at Telica volcano (Nicaragua). *J. Volcanol. Geotherm. Res.* **341**, 131–148 (2017).

87. P. Robidoux, M. L. Frezzotti, E. H. Hauri, A. Aiuppa, Shrinkage Bubbles: The C–O–H–S Magmatic Fluid System at San Cristóbal Volcano. *J. Petrol.* **59**, 2093–2122 (2018).

88. C. M. Allison, *Highly Explosive Mafic Volcanism: The Role of Volatiles* (Arizona State University, 2018).

89. E. Bali, M. E. Hartley, S. A. Halldórsson, G. H. Gudfinnsson, S. Jakobsson, Melt inclusion constraints on volatile systematics and degassing history of the 2014–2015 Holuhraun eruption, Iceland. *Contrib. Mineral. Petrol.* **173**, 9 (2018).

90. E. N. Bennett, F. E. Jenner, M.-A. Millet, K. V. Cashman, C. J. Lissenberg, Deep roots for mid-ocean-ridge volcanoes revealed by plagioclase-hosted melt inclusions. *Nature* **572**, 235–239 (2019).

91. E. Gennaro, G. Iacono-Marziano, A. Paonita, S. G. Rotolo, C. Martel, A. L. Rizzo, M. Pichavant, M. Liotta, Melt inclusions track melt evolution and degassing of Etnean magmas in the last 15 ka. *Lithos* **324–325**, 716–732 (2019).

92. M. Manzini, A.-S. Bouvier, L. P. Baumgartner, E. F. Rose-Koga, P. Schiano, N. Shimizu, Grain scale processes recorded by oxygen isotopes in olivine-hosted melt inclusions from two MORB samples. *Chem. Geol.* **511**, 11–20 (2019).

93. W. G. R. Miller, J. Maclennan, O. Shorttle, G. A. Gaetani, V. Le Roux, F. Klein, Estimating the carbon content of the deep mantle with Icelandic melt inclusions. *Earth Planet. Sci. Lett.* **523**, 115699 (2019).

94. Z. Taracsák, M. E. Hartley, R. Burgess, M. Edmonds, F. Iddon, M.-A. Longpré, High fluxes of deep volatiles from ocean island volcanoes: Insights from El Hierro, Canary Islands. *Geochim. Cosmochim. Acta* **258**, 19–36 (2019).

95. F. Iddon, M. Edmonds, Volatile-Rich Magmas Distributed Through the Upper Crust in the Main Ethiopian Rift. *Geochem. Geophys. Geosystems* **21**, e2019GC008904 (2020).

96. C. M. Allison, K. Roggensack, A. B. Clarke, Highly explosive basaltic eruptions driven by CO2 exsolution. *Nat. Commun.* **12**, 217 (2021).

97. A. Hernandez Nava, B. A. Black, S. A. Gibson, R. J. Bodnar, P. R. Renne, L. Vanderkluysen, Reconciling early Deccan Traps CO2 outgassing and pre-KPB global climate. *Proc. Natl. Acad. Sci.* **118**, e2007797118 (2021).

98. D. J. Rasmussen, T. Plank, Melt inclusion data for the central-eastern Aleutian volcanoes, EARTHCHEM (2021); https://doi.org/10.26022/IEDA/111873.

99. M. L. M. Gleeson, S. A. Gibson, M. J. Stock, Constraints on the behaviour and content of volatiles in Galápagos magmas from melt inclusions and nominally anhydrous minerals. *Geochim. Cosmochim. Acta* **319**, 168–190 (2022).

100. K. Wong, D. Ferguson, P. Wieser, D. Morgan, M. Edmonds, A. Z. Tadesse, G. Yirgu, J. Harvey, S. Hammond, Focused Mid-Crustal Magma Intrusion During Continental Break-Up in Ethiopia. *Geophys. Res. Lett.* **50**, e2023GL103257 (2023).

101. M. S. Ghiorso, G. A. R. Gualda, An H2O–CO2 mixed fluid saturation model compatible with rhyolite-MELTS. *Contrib. Mineral. Petrol.* **169**, 53 (2015).

102. K. Iacovino, S. Matthews, P. E. Wieser, G. M. Moore, F. Bégué, VESIcal Part I: An Open-Source Thermodynamic Model Engine for Mixed Volatile (H2O-CO2) Solubility in Silicate Melts. *Earth Space Sci.* **8**, e2020EA001584 (2021).

103. R. T. Helz, C. R. Thornber, Geothermometry of Kilauea Iki lava lake, Hawaii. *Bull. Volcanol.* **49**, 651–668 (1987).

104. P. Wieser, M. Petrelli, J. Lubbers, E. Wieser, S. Ozaydin, A. Kent, C. Till, Thermobar: An open-source Python3 tool for thermobarometry and hygrometry. *Volcanica* **5**, 349–384 (2022).

105. K. D. Putirka, Thermometers and barometers for volcanic systems. *Rev. Mineral. Geochem.* **69**, 61–120 (2008).

106. P. Beattie, Olivine-melt and orthopyroxene-melt equilibria. *Contrib. Mineral. Petrol.* **115**, 103–111 (1993).

107. P. E. Wieser, M. Gleeson, S. Matthews, C. L. DeVitre, E. Gazel, Determining the Pressure – Temperature – Composition (P-T-X) conditions of magma storage. (2023).